ResearchGate

See discussions, stats, and author profiles for this publication at: https://www.researchgate.net/publication/229307748

Ultrafast studies of shock waves using interferometric methods and transient infrared absorption spectroscopy

ARTICLE *in* THIN SOLID FILMS · APRIL 2004

Impact Factor: 1.76 · DOI: 10.1016/j.tsf.2003.11.116

CITATIONS
13

READS
62

9 AUTHORS, INCLUDING:

D. J. Funk
Los Alamos National Laboratory
133 PUBLICATIONS **1,488** CITATIONS
SEE PROFILE

David S. Moore
Los Alamos National Laboratory
188 PUBLICATIONS **2,339** CITATIONS
SEE PROFILE

Shawn Mcgrane
Los Alamos National Laboratory
76 PUBLICATIONS **500** CITATIONS
SEE PROFILE

Jeffrey W Nicholson
OFS Fitel Denmark
214 PUBLICATIONS **2,743** CITATIONS
SEE PROFILE

Available from: Jeffrey W Nicholson
Retrieved on: 26 January 2016

Available online at www.sciencedirect.com
SCIENCE DIRECT®
Thin Solid Films 453–454 (2004) 542–549
thin solid films
www.elsevier.com/locate/tsf

Ultrafast studies of shock waves using interferometric methods and transient infrared absorption spectroscopy

D.J. Funk[a,*], D.S. Moore[a], S.D. McGrane[a], K.T. Gahagan[a,b], J.H. Reho[a,c], S.J. Buelow[a], J. Nicholson[a,d], G.L. Fisher[a], R.L. Rabie[a]

[a]*Materials Dynamics Group, DX-2, Los Alamos National Laboratory, Los Alamos, NM 87545, USA*
[b]*Corning, Incorporated, Corning, NY 14831, USA*
[c]*East Carolina University, Greenville, NC 27858-4353, USA*
[d]*Lucent Technologies, Murray Hill, NJ, USA*

Abstract

During the past few years, we have set up two ultrafast laboratories to study laser-induced shock waves with picosecond (or better) temporal resolution. In this paper, we provide an overview of our laboratories and the diagnostics we have developed to study the dynamic processes of matter being shocked to extreme conditions. Results are presented on the measurement of the shock wave rise time in aluminium and nickel, the effects of dynamic pressure on the complex index in aluminium, the measurement and characterization of the shock velocity, particle velocity, and index of refraction in shocked polymethylmethacrylate (PMMA), and our initial studies of transient infrared vibrational spectroscopy of shocked energetic polymers (nitrocellulose and poly-vinyl nitrate).
© 2003 Elsevier B.V. All rights reserved.

Keywords: Shock waves; Infrared spectroscopy; Optical properties; Aluminium; Nickel; Interferometry

1. Introduction

A molecular description of detonation has been pursued for decades [1], with little or no success in obtaining high-quality data at these scales. Recently, we have setup laboratories specifically designed to address this deficiency, employing pump-probe techniques based on chirped-pulse amplified Ti:sapphire laser technology coupled with thin film targets of energetic materials [2]. Several reasons exist for these technological choices, including the relative ease of synchronicity that one can obtain using direct optical drive followed by optical probe. In contrast to shock experiments with gas guns in which obtaining synchronicity to a few picoseconds is extremely difficult and time-resolution occurs with fast streak cameras, optical synchronicity is simply obtained by changing the optical path lengths with translation stages and the time resolution results from the 130 fs 'frames' that are recorded as a function of delay. In addition, these timescales are required if one would like to resolve the 'rise time' (e.g. ambient to peak pressure) of the shock wave, observe energy transfer and/or redistribution within the shock wave (phonons, molecular vibrations), observe shock-induced chemical reactions, or study some shock-induced phase transitions (solid–solid and solid–melt). For example, a shock wave propagating through a material at a velocity of 6 km/s causes the material to 'jump' to a velocity of 1 or 2 km/s. Such a 'particle velocity' translates to a time and distance scale of 2 μm/ns or 2 nm/ps. Consequently, if one is to time-resolve the processes listed above at these scales, one needs picosecond or better temporal resolution. Furthermore, these 'table-top' experiments are generated in small sample areas (0.03 mm^2) and can be conducted repetitively, achieving very high S/N ratios that cannot be readily obtained in single-shot experiments. Due to the high intensity of the amplified ultrafast laser pulses, it is quite easy to generate a variety of probe wavelengths, making the technique spectroscopically versatile: transient experiments using Raman, IR absorption, UV–Vis absorption, or CARS can easily be conducted. However, there was concern that these methodologies would not

*Corresponding author. Tel.: +1-505-667-9659; fax: +1-505-667-6372.
E-mail address: djf@lanl.gov (D.J. Funk).

0040-6090/04/$ - see front matter © 2003 Elsevier B.V. All rights reserved.
doi:10.1016/j.tsf.2003.11.116

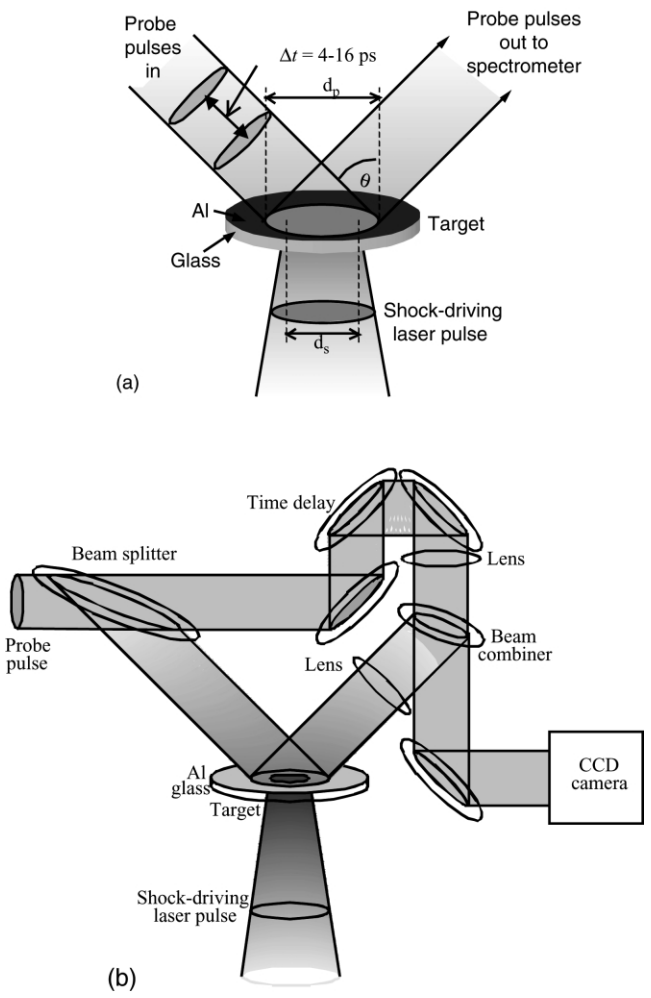

Fig. 1. Schematic diagrams of the femtosecond laser-driven shock interferometry experiments: (a) frequency domain interferometry and (b) ultrafast two-dimensional spatial interferometric microscopy.

yield conditions in the shocked materials that would allow interpretable results. We have conducted a number of characterization experiments of our shock waves using interferometric methods that have supported our choice of technology and have led to the results presented here, ultimately leading to the first observation of shock-induced chemistry in an energetic material on picosecond time-scales.

2. Experimental

2.1. Interferometric measurements

In the experiments described here, two separate techniques are used for interferometric characterization of the shocked material's motion: frequency domain interferometry (FDI) [3–6] and ultrafast spatial interferometric microscopy [7]. Shown in Fig. 1a, is our implementation of reflection frequency domain interferometry. Here, a pair of ultrafast probe pulses is used to simultaneously measure the dynamic phase shift and reflectance during shock breakout from thin-film metal targets. For the FDI experiments, a single 800 nm, $t_p =$ 130 fs, 0.7 mJ laser pulse generated by a seeded, chirped pulse amplified Ti:sapphire laser system (Spectra Physics) was used for both shock-generation and probing. The shock generating pulse (0.2–0.5 mJ) was focused onto the front side of the target assembly to a spot size of $d_s = 75$ μm. A small portion of the main pulse (approx. 0.04 mJ) reflected from a beam splitter was passed through an unbalanced Michelson interferometer to produce a pair of probe pulses separated in time by 4–16 ps. These *s*-polarized pulses were loosely focused onto the backside of the target at an angle of $\theta = 32.6°$ to a spot size of ~200 μm to circumscribe the region of shock breakout at probe intensity less than $\sim 5 \times 10^{11}$ W/cm^2 (pump intensity of approx. 1×10^{14} W/cm^2). The reflected probe pulses were imaged at ×16 magnification onto the entrance slit of a high resolution imaging spectrograph (Acton model 300i) with TE-cooled CCD detector (Photometrics model SenSys 1600). Following Giendre et al. [7], the relative phase shift between the probe pulses caused by motion of the free surface and/or transient changes in the optical properties of the surface during shock breakout was determined by performing an inverse fast-Fourier transform (IFFT) on the spectral intensity interferogram recorded on the spectrograph CCD as in [6]. The dynamic phase and reflectance are extracted from the analysis using baseline fitting to the unshocked region surrounding the shock breakout region.

Shown in Fig. 1b is a schematic of the setup for ultrafast spatial interferometric microscopy. Here, a small portion of the main laser pulse (approx. 10 μJ) is reflected from a beam splitter and passed through a modified Mach–Zehnder interferometer with the sample in one arm (the sample arm) and a variable delay, to control temporal overlap, in the other (reference) arm. The probe pulse in the sample arm was focused onto the target at an incidence angle of either 32.6 or 76.0° to a spot size of ~1000 μm to circumscribe the optically pumped region. For these studies, the probe pulse was *p*-polarized relative to the plane of incidence. A lens was used to image the surface (at approx. 2 pixels/μm) onto a CCD camera (same camera as above). A duplicate imaging lens was used in the reference arm. The sample and reference arms were recombined at a slight angle to produce an interference pattern on the CCD. This interferogram was transferred to and stored in a computer, and all interferograms from a time series, built up by adjusting the time delay in the shock driving laser arm, were post processed off line. In practice, three images were obtained at 1 Hz: (a) a 'reference' interferogram, I_r, taken before the pump pulse arrives, (b) a 'pump' interferogram, I_p, taken 'during' the experiment and, (c) a post-shot interferogram to observe the damage

to the material after the experiment. Analysis is conducted using the FFT method first developed by Takeda [8], and described in [7]. Two two-dimensional data maps are constructed, one containing the amplitude or reflectivity information, the other containing the phase information, which is composed of optical property and surface position data. Each time data point is obtained by averaging the two-dimensional map values in an area that is approximately 20 μm in diameter at the center of each laser experiment.

2.2. Transient infrared spectroscopy

For these studies, in addition to the interferometric measurements, time-dependent infrared absorption measurements were also made. Tunable mid-IR output from an optical parametric amplifier (OPA; Spectra Physics), pumped by a small portion (approx. 1 mJ) of the main femtosecond laser beam, was split into two beams, a sample and reference. The sample laser beam was directed on and focused to a ~45 μm spot that intersected the center area of the sample to be shocked. For these experiments, a spectrally modified and temporally stretched driving pulse was used to generate the shock waves; choice of this pulse format yielded high-pressure (approx. 200 kbar), sustained (approx. 250 ps) shock waves in the energetic films [9]. The reflected IR laser beam was then directed through a 0.125 m IR spectrometer (Oriel, 75 lines/mm grating blazed at 7 μm) onto the upper half of a 256×256 HgCdTe focal plane array (FPA) cooled to liquid N_2 temperatures. Similarly, the reference arm was also directed through the IR spectrometer and collected on the lower half of the FPA. Spectral calibration was performed through use of 'air' absorptions observed in the spectra [10], and the transmission was calculated by taking the ratio of the spectrum from the sample arm (divided by the spectrum from an aluminium reference target) to the reference arm (also divided by the spectrum from an aluminium reference target). Time-dependent spectra were obtained as above, by delaying the pump (shock driving) beam relative to the probe.

2.3. Targets studied

The metal targets used in these experiments were Al and Ni films of varying thickness produced by vapor deposition onto 150±20-μm thick BK-7 microscope cover slips (Fisher Scientific). The samples were examined both with a spectroscopic ellipsometer (Sentech SE 800) and an atomic force microscope (AFM; Quesant Nomad). Best fits to the spectral ellipsometric data from a 750 nm Al sample (Ψ and Δ measured over 400–840 nm) modeled as an Al_2O_3 layer on top of the aluminium substrate yielded an Al_2O_3 layer 4.9-nm thick, consistent with literature results [11]. AFM results indicated an RMS roughness of ~5 nm over a 900 μm^2 area, consistent with the ellipsometric data, in which Ψ was fit less satisfactorily than Δ. Polymethylmethacrylate (PMMA), nitrocellulose (NC; 12.6% N), and polyvinylnitrate (PVN 14.5% N) films were spin coated from the appropriate solutions (toluene or 'magic' solvent), on to 500–1000 nm thick aluminium films described above. Concentration of the solution was used to control film thickness. Thickness and surface uniformity of the films were monitored with null ellipsometry (Rudolph Research, AutoEL) at helium neon wavelength, 70° incidence, and using white light reflectometry spectral interference fringe analysis (Filmetrics). Both methods of film thickness measurement are sensitive to changes as small as a nanometer, and the best films produced have surface thickness variations of 1% across most of a 2-cm diameter sample. In all experiments, the targets were mounted on a computer-controlled x–y translation stage (where z was the normal to the target surface). The target was rastered at ~300 μm intervals between pump pulses so that each 'experiment' involved undisturbed material.

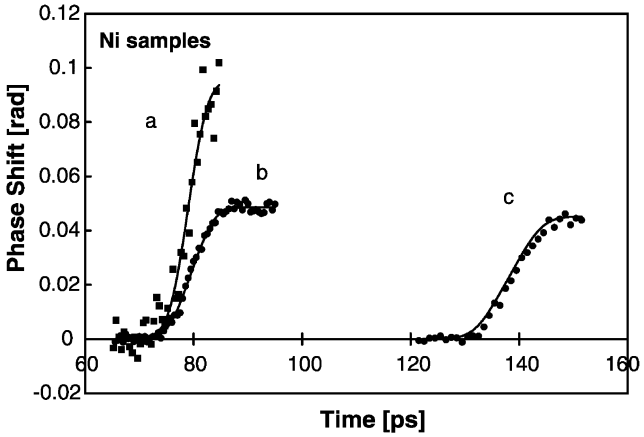

Fig. 2. Plot of relative phase difference between the probe beams vs. relative delay (to the pump laser) for a shock wave breakout from three nickel films. (a) 467 nm film probed at $\lambda = 400$ nm, $\Delta t = 6$ ps, (b) 467 nm film probed at $\lambda = 800$ nm, $\Delta t = 8$, and (c) 839 nm film probed at $\lambda = 800$ nm, $\Delta t = 8$ ps.

3. Results and discussion

3.1. Shock wave rise time measurements

Thin nickel and aluminium films were shocked using ~0.5 mJ of the output of the 800 nm laser [6]. FDI was used to measure the phase shift caused by the shocked material's free surface motion, yielding the acceleration and final velocity of shocked Al and Ni thin films. Fig. 2 shows the relative phase shift, $\Delta\phi$, as a function of pump delay time for three nickel films: (a) a 467 nm film probed at $\lambda = 400$ nm, $\Delta t = 6$ ps, (b)

a 467 nm film probed at $\lambda = 800$ nm, $\Delta t = 8$, and (c) an 839 nm film probed at $\lambda = 800$ nm, $\Delta t = 8$ ps. The targets were each fabricated with a thin (50 nm) region to be used as a fiducial for measuring the shock breakout time relative to initiation, from which the average shock velocity through the sample was determined. Time $t = 0$ in Fig. 2 corresponds to the estimated arrival of the laser pulse at the nickel surface. All three samples exhibit a phase profile consistent with that expected for a sharp, but finite width shock. The phase profile of such an idealized discontinuous (zero rise time) shock front would be characterized by an *instantaneous* transition from the initial $\Delta\phi = 0$ value (when both probe pulses arrive before the shock), to a region of linear rise for the length of the time separation between the probe pulses (i.e. only the trailing probe pulse sees the surface moving at constant velocity), followed by a second *instantaneous* change to a constant $\Delta\phi$ proportional to the free surface velocity (both pulses arrive after the shock and see a constant surface velocity). The measured phase profiles exhibit similar characteristics, but with smooth rather than instantaneous transitions on the time scales of the measurement, indicative of an observable acceleration of the free surface. To obtain a particle velocity and shock wave rise time, we assume a hyperbolic tangent form for the free surface velocity, $u_{fs}(t) = u_p[1 + \tanh((t - t_0)/\tau_{fs})]$, where τ_{fs}, and t_0 are fitting parameters characterizing the free surface velocity profile. The final free surface velocity is taken to be twice the final particle velocity of the shock state, $u_{fs}(t \gg t_0) = 2u_p$ and assumes a reflected Hugoniot or Walsh equation of state for the rarefaction wave. Extracting a shockwave pressure profile from the measured free surface velocity is not straightforward. The principle difficulty lies in determining the relative timing between the arrival of the shock wave at the surface and the development of the rarefaction wave passing back into the material. In one limit, we may imagine that the two events occur simultaneously. That is, as the shock pressure rises incrementally, the rarefaction develops and the free surface accelerates to the velocity corresponding to isentropic relaxation from the shock state. In this case, we may approximate the time-dependent particle velocity as half the free surface velocity $u_p(t) = u_{fs}(t)/2$ Thus, the free surface velocity, particle velocity and shock velocity are all characterized by the single time

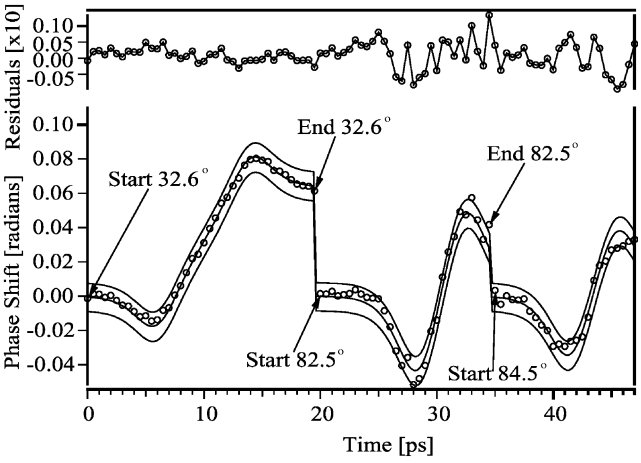

Fig. 3. Plot of measured phase difference between the probe beams vs. relative delay (to the pump laser) for a shock wave breakout from a 750 nm thick Al thin film. The probes are *p*-polarized 800 nm light taken at three angles of incidence (which are offset in time for clarity). Note the maximum negative phase difference occurs in the data taken near the quasi-polarizing angle in aluminium (82.5°). The dashed lines are 95% confidence limit prediction bands.

constant τ_{fs}. Defining the shock wave rise time as the 10–90% width of the hyperbolic tangent rise gives $\tau_{sh} = 2.3\tau_{fs}$. Values of τ_{sh} are reported in Table 1 for aluminium and nickel films and were found to be 5–6 ps. We have also conducted experiments to investigate the effect of surface roughness by probing through the glass layer where the interface roughness is much smaller than at the free surface of a vapor deposited film. We found no measurable difference in the rise time. The short rise times we measure suggest that the thickness of these shocks is tens of lattice spacings. These results are larger than, but comparable with, molecular dynamics simulations of shocks in other metals (e.g. [12]) and may have implications for reaction chemistry in energetic materials under similar shock loading conditions, such as direct pumping into transition states.

3.2. Shock-induced changes in the complex index

Fig. 3 shows three sets of FDI measurement of the relative phase shift as a function of delay time between the shock generation pulse and the probe pulses for a 750-nm thick Al film [13]. All data were taken with an

Table 1
Extracted fitting parameters. See text for details

Sample	λ_{pr} (nm)	$\bar{u}_{sh}$ (nm/ps)	u_{sh} (nm/ps)	u_p (nm/ps)	τ_{fs} (ps)	τ_{sh} (ps)
1000 nm Al	400	–	5.72 ± 0.02	0.291 ± 0.016	2.32 ± 0.40	5.34 ± 0.92
467 nm Ni	800	6.62 ± 0.40	4.93 ± 0.01	0.23 ± 0.01	2.54 ± 0.73	5.84 ± 1.68
839 nm Ni	800	6.15 ± 0.39	4.93 ± 0.02	0.231 ± 0.014	2.71 ± 1.10	6.23 ± 2.53
467 nm Ni	400		5.03 ± 0.06	0.30 ± 0.04	2.57 ± 1.42	5.91 ± 3.24

Table 2
Parameters yielded by non-linear least squares analysis and comparison to literature values

	This work, 800 nm 4.65 GPa	This work, 400 nm	4.65 Gpa [19,20]	Ambient [16,17]	UHV [11]
τ	2.36 ± 0.09 ps	2.32 ± 0.40 ps			
u_p	0.300 ± 0.006 nm/ps	0.29 ± 0.02 nm/ps			
n	1.56 ± 0.20		1.79	2.35	2.798
k	8.29 ± 0.04		6.68	7.80	8.446

800 nm *p*-polarized probe but at different angles of incidence and temporal separations (32.6°, 8 ps; 82.5°, 4 ps; 84.5°, 4 ps). The *negative* phase shift that occurs during shock breakout is very apparent and unexpected (we use the convention in our data analysis that material motion alone would yield a *positive* phase shift). We have also conducted experiments with the identical sample under similar conditions, but with a probe wavelength of 400 nm and probe pulse separation of 4 ps. No experiment done with the probe wavelength at 400 nm resulted in an observable negative phase shift during shock breakout.

Reflection from an air–metallic interface is governed by Maxwell's equations and the appropriate boundary conditions leading to the Fresnel relations for the reflection amplitudes of *s*- and *p*-polarized light. Thus, upon reflection from a stationary metallic surface, the electric field undergoes a phase shift, ϕ_n, with magnitude r_n, that can be accurately calculated from knowledge of the complex index of refraction, polarization state, and the angle of incidence of the light striking the sample. Moreover, this phase shift will be influenced by any time-dependent changes in the complex index of refraction of the material. Thus, we hypothesize that the differences in the *p*-polarized 800 nm probe data and the 400 nm probe data are due to differences in the measured phase shifts, resulting from the pressure-induced shift of the U(200) interband transition in aluminium. To quantify the influence of changes in the complex index, we modeled the data of Fig. 3. Measurement at incident angles near the quasi-polarizing angle (near 82.5° in aluminium) minimized the contribution of the phase signal due to surface motion, which is proportional to the cosine of the angle of incidence (cf. Eq. (1)), and maximized the effect of the complex index changes. We took the changes in the complex index to be proportional to the acceleration of the surface, which is related to the pressure. To extract an *n*-effective (n_{eff}) and *k*-effective (k_{eff}), and to account for the Al_2O_3 over-layer in phase shift calculations, we treated the over-layer/aluminium as a thin film in which *only* the complex index of the aluminium is time-dependent. We set the index of the Al_2O_3 layer ($n=1.76$, $k=0$) to literature values [14] and we fixed the layer thickness at 4.9 nm. This choice is consistent with the fact that the index of sapphire changes very little under moderate shock conditions (<12.0 GPa) [15], and that the compression the sapphire undergoes due to the shock wave (less than 2% or 0.1 nm) causes a phase shift less than the noise in our method (0.7 nm RMS [9]). The three data sets were fit simultaneously to the differences of the following equation for the time-dependent phase shift of each probe:

$$\phi_{\mathrm{j}}(t) = \Delta\phi_{n,n_{\mathrm{eff}},k,k_{\mathrm{eff}}}\mathrm{sech}^2\left(\frac{t-t_{\mathrm{j}}+\delta t_{\mathrm{j}}}{\tau}\right) + \frac{4\pi\cos(\theta_{\mathrm{o}})}{\lambda_{\mathrm{o}}}\int_{t_{\mathrm{i}}}^{t_{\mathrm{f}}} u_p\left(1+\tanh\left(\frac{t-t_{\mathrm{j}}+\delta t_{\mathrm{j}}}{\tau}\right)\right)\mathrm{d}t, \quad (1)$$

where ϕ_{j} is the phase shift for probe pulse j, $\Delta\phi$ is determined by taking the difference in phases using the appropriate Fresnel coefficients, and λ_{o} is the wavelength. δt_{j} is determined from the temporal delay introduced by the interferometer. The following parameters were varied: τ, u_{p}, t_{j}, n_{eff}, k_{eff}, where τ is the hyperbolic tangent time constant, u_{p} is the shock state particle velocity, t_{j} are offsets for the data from each set (time relative to the pump, which can change from day to day) and n_{eff} and k_{eff} are the effective complex index of shocked aluminium. Non-linear least squares analysis yielded the parameters in Table 2. Also listed are the *n* and *k* calculated from Sturm and Ashcroft's model [16], with the modified parameters introduced in [17] affected by the shift in position of U(200). We note that the absolute magnitudes of the changes in the complex index are different, but the trends are in the correct direction. Thus, we conclude that our data are being influenced by the pressure-dependent shift of the U(200) interband transition in aluminium, and its effect on the complex index. Finally, we have also taken data with nickel substrates (Fig. 4) at three angles of incidence [13]. In the case of nickel, we found the observed optical contributions are of the opposite sign as those for aluminium, indicating that the nickel data taken at 32.6° contain an optical phase contribution in the same direction as surface motion. However, in contrast to aluminium, this may be interpretable in terms of a Drude

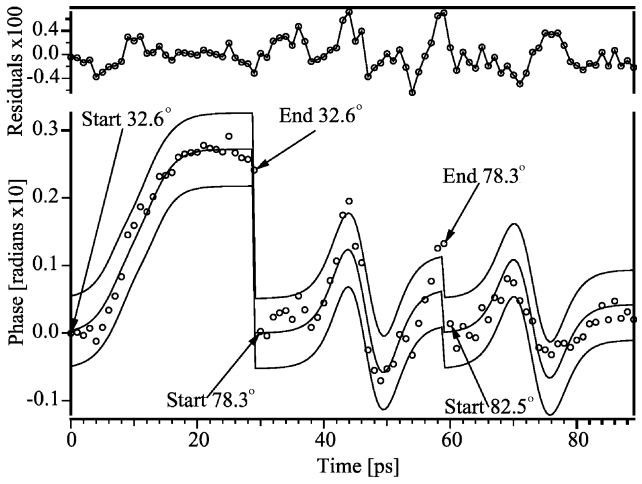

Fig. 4. Plot of measured phase difference between the probe beams vs. relative delay (to the pump laser) for shock wave breakout from a 500 nm thick Ni thin film. The data were obtained using *p*-polarized 800 nm light and taken at three angles of incidence (which are offset in time for clarity). Note the large positive phase difference in the data taken near the quasi-polarizing angle in nickel (78.3°), indicating significant complex index changes leading to phase differences of the same sign as those from surface motion. The dashed lines are 95% confidence limit prediction bands.

response, as nickel has no interband transition near 800 nm. We note that the absolute position of the surface derived from these measurements *would be in error* if the optical effects were not taken into account.

3.3. Sub-picosecond interferometry of shocked PMMA films

Shown in Fig. 5 are the measured (using ultrafast spatial interferometric microscopy) time-dependent phase shifts of a 625 nm PMMA film acquired using *s* and *p* polarization at both 32.6° and 76.3° angles of incidence [18]. The solid lines are fits to the surface motion, $u_p = 2.45$ km/s, and the dashed and dotted lines represent fits for *s* and *p* polarization, respectively, of the phase shift including the interference effects (see below). The shock velocity, $U_s = 6.5$ km/s was also found from the fit and using the PMMA density of 1.186 g/cm^3 [19], we calculate the pressure in the PMMA to be 19 GPa. Note that all data shown are recorded prior to the shock completely traversing the film to avoid complications of the PMMA surface release.

To determine the effect of the weakly reflective shock wave and allow modeling of the data, the expected behavior of the thin film was constructed as shown in Fig. 6, consisting of the following layers: (1) 500 nm aluminium, (2) 4 nm Al_2O_3, (3) time-dependent layer of shocked PMMA $[d(t) = (U_s - u_p)t]$, and (4) unshocked PMMA $[l(t) = d_o - U_s t]$. The Fresnel coefficient for

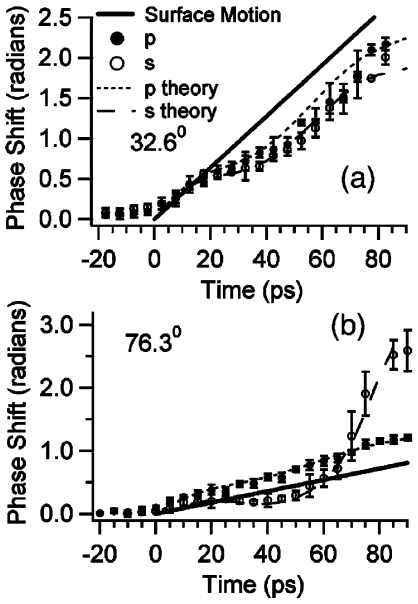

Fig. 5. Phase shifts for 625 nm PMMA on Al during shock. Solid lines are fits to surface motion phase shifts, determining $u_p = 2.45$ km/s, $U_s = 6.5$ km/s ($P = 19$ GPa), and $n_{shocked} = 1.77$, Dotted (*p*-polarization) and dashed (*s*-polarization) lines are calculated including thin film interference. Experimental points are, ○, *p* and ●, *s* polarization at (a) 32.6° and (b) 76.3°.

reflection from the thin film was calculated using standard matrix formalism [20]. This coefficient was then written in the form as $r = |r|\exp(i\phi)$, where r is the reflection amplitude and ϕ is the phase shift, and the change in phase calculated as the difference in the phase shift expected from the ambient film and that from shocked film for the proper angle of incidence and polarization. A best fit was obtained to all four data sets by varying u_p, U_s and $n_{shocked}$ and invoking the following assumptions: a constant u_p, and negligible contribution

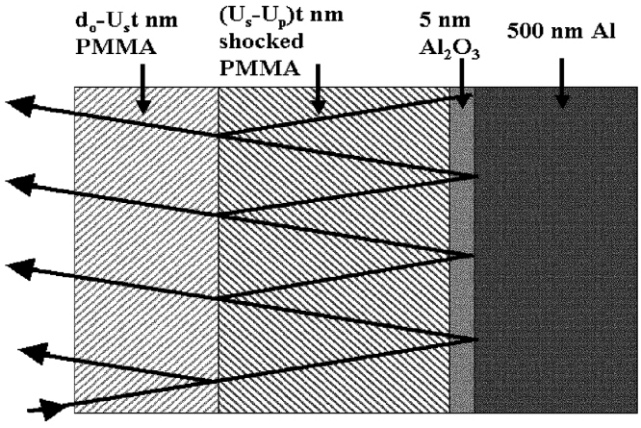

Fig. 6. Diagram of thin film structure and time-dependent thicknesses as shock transits sample from right to left. Shock velocity is U_s and Al interface velocity is u_p. Arrows indicate path of light partially reflected off interfaces, leading to thin film interference.

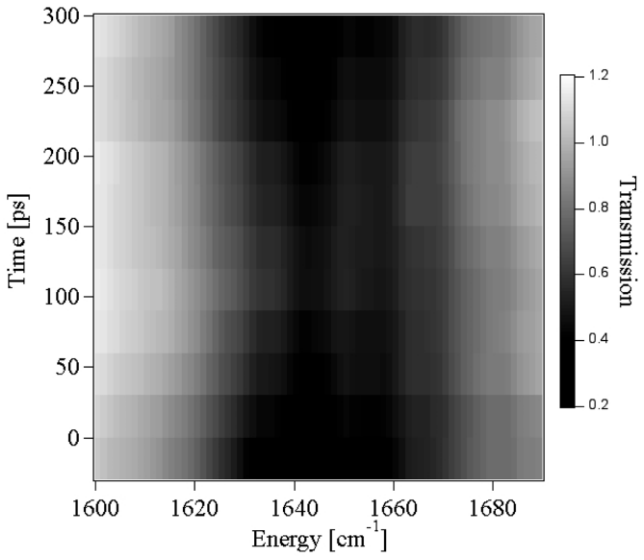

Fig. 7. A plot of infrared transmission vs. energy near the asymmetric stretching frequency in NC, for a series of pump-probe delays (shock wave pressure approx. 200 kbar). Each spectrum consists of an average of three shots. Initially, the absorption decreases with time, but recovers at long times (315 ps) indicating that the NC does not undergo reaction.

to phase shift from shock heated Al and PMMA [21]. The fit obtained with these assumptions matches the data within the experimental error, as shown in Fig. 5, implying the assumptions made are applicable in this regime. The fitted $n_{\text{shocked}} = 1.77$ compares favorably with that calculated using the Gladstone–Dale approximation, $n_{\text{shocked}} = 1.79$ [22,23], which has been shown to be valid in this pressure regime.

The plot of 'true' surface motion extracted from the fit and plotted in Fig. 5 indicates that shock interferometry experiments with thin film transparent materials cannot measure the motion of the reflective surface directly because of thin film interference effects. These interference effects arise from multiple reflections of the interferometry probe laser pulse within the shocked and unshocked thin film layers due to their different indices of refraction. The interference effects change as each layer thickness changes with shock transit through the film. Therefore, thin film shock interferometry experiments must deconvolve the surface motion from the thin film interference, which can be accomplished by repeating measurements at two angles of incidence and two polarizations. A simple model of the shock process coupled with implementation of thin film interference equations allowed calculation of these effects. PMMA films shocked to 19 GPa matched the theoretical predictions within experimental error, justifying a number of assumptions made in modeling the data: that the particle velocity produced by our shocks is nearly constant, that the Gladstone–Dale model for shocked refractive index is valid here, that heating of the sample introduces negligible phase shift, and that the thin film Hugoniot is essentially equal to that of the bulk material. These results support the relevance of short time, small length scale measurements for increasing understanding of larger scale shock phenomenon.

3.4. Shock-induced chemical reaction of energetic polymers

Shown in Fig. 7 are the time-dependent IR transmission spectra obtained near the asymmetric nitro stretching frequency of NC shocked to ~200 kbar. As observed in the figure, the absorption decreases in intensity and is slightly blue-shifted, but recovers very nearly completely at long times. In fact, a plot of ΔA (absorbance) vs. time indicates that the absorption changes linearly, consistent with one might expect for the traversal of a shock wave through the material at a constant velocity. However, and quite surprisingly, this also indicates that little or no reaction has occurred under these conditions for this shock-loaded material. In the figure, the shock has reached the free surface at approximately 150 ps and the sample starts to unload through propagation of a rarefaction wave back into the material at this time [24]. In contrast, Fig. 8 shows a similar plot, this time of the time-dependent IR transmission spectra obtained near the symmetric nitro stretching frequency of PVN, also shocked to ~200 kbar. In this plot, we also observe a blue shift, but in addition, we observe a significant loss of absorption as

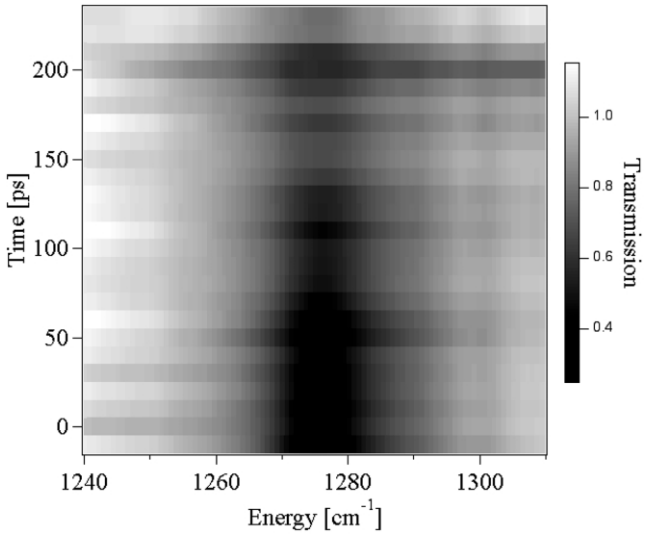

Fig. 8. A plot of infrared transmission vs. energy near the symmetric stretching frequency in PVN, for a series of pump-probe delays (shock wave pressure approx. 200 kbar). Each spectrum consists of an average of three shots. In contrast to the NC, the PVN absorption continually decreases with pump-probe delay and never recovers, indicating complete reaction of the material.

a function of time with very little, if any, recovery at long time. We attribute this result to reaction of the PVN nearly immediately following the passage of the shock wave. We are presently modeling this data and conducting additional experiments to understand this behavior. Why do we observe such different behavior between these two polymers? Presently, we are discussing the hypothesis that one of the polymers (PVN) is much more crystalline than the other, leading to the possibility of shear-induced reaction occurring in this polymer. Static infrared absorption spectroscopy supports this notion [25]; the spectroscopic lines observed are less inhomogenously broadened for PVN than NC, but much more work needs to be done before we can assert this conclusion.

4. Conclusions

Much of the research discussed above was conducted in preparation for the studies that examined shock-induced chemistry in energetic materials. The knowledge we obtained regarding the influence of direct laser-drive upon the target on which the energetic polymer was coated, has led to our confidence that the reaction chemistry studies provide relevant information regarding the first decomposition steps in shock-loaded energetic materials. For example, the PMMA interferometric data were well-modeled using the bulk Hugoniots of both the PMMA and the aluminium; thus, the use of direct-drive did not perturb the thermodynamic state significantly from the Hugoniot, allowing us to make the assumption that on these timescales (hundreds of picoseconds), the states are well-approximated as the same relevant state obtained with gas-gun systems. We have also shown that caution must be exercised when attempting to use the interferometric data for the characterization of material motion: changes in the material properties can influence the interferometric data and must be deconvolved to yield the 'true' surface motion. However, this also offers the possibility of using the changes in material properties as a measure of the shocked material's thermodynamic state: discontinuities will exist in the index of refraction as the material crosses a phase boundary. These changes may then be used as a characterization tool if they are accurately measured using the interferometric techniques, to measure phase boundaries under shock-loaded conditions. Finally, we have shown that two energetic polymers, both shocked to $\sim$200 kbar, exhibit completely different behavior: in one case (NC), the material exhibits no indication of chemical reaction, even at long times, when the heating of the metal target from the laser pulse might become important. In stark contrast to this result, we observe a disappearance of the symmetric stretch in shocked PVN, indicating significant reaction as the shock wave traverses the film.

Acknowledgments

This work was performed at Los Alamos National Laboratory by the University of California under the auspices of the Department of Energy under contract W-7405-ENG.

References

[1] See, for example, C.M. Tarver, J. Phys. Chem. 101(27) (1997) 4845 and references therein.
[2] Our scheme closely resembles that in D.E. Hare, J. Franken, D.D. Dlott, Chem. Phys. Lett. 244(3–4) (1995) 224–230.
[3] E. Tokunaga, A. Terasaki, T. Kobayashi, Opt. Lett. 17 (1992) 1131.
[4] J.P. Geindre, P. Audebert, A. Rousse, F. Falliès, J.C. Gauthier, A. Mysyrowicz, A. Dos Santos, G. Hamoniaux, A. Antonetti, Opt. Lett. 19 (1994) 1997.
[5] R. Evans, A.D. Badger, F. Failliès, M. Mahdieh, T.A. Hall, P. Audebert, J.-P. Geindre, J.-C. Gauthier, A. Mysyrowicz, G. Grillon, A. Antonetti, Phys. Rev. Lett. 77 (1996) 3359.
[6] K.T. Gahagan, D.S. Moore, D.J. Funk, R.L. Rabie, S.J. Buelow, J.N. Nicholson, Phys. Rev. Lett. 85 (15) (2000) 3205–3208.
[7] K.T. Gahagan, D.S. Moore, D.J. Funk, J.H. Reho, R.L. Rabie, J. Appl. Phys. 92 (7) (2002) 3679–3682.
[8] M. Takeda, H. Ina, S. Kobayashi, J. Opt. Soc. Am. 72 (1982) 156–160.
[9] S.D. McGrane, D.S. Moore, D.J. Funk, R.L. Rabie, Appl. Phys. Lett. 80 (2002) 3919.
[10] This is true for the 1650 cm^{-1} region; the calibration was assumed to be linear in the 1280 cm^{-1} region (constant energy/pixel).
[11] D.Y. Smith, E. Shiles, M. Inokuti, in: E.D. Palik (Ed.), Handbook of Optical Constants of Solids, Academic Press, San Diego, 1985, p. 374.
[12] K. Kadau, T.C. Germann, P.S. Lomdahl, B.L. Holian, Science 296 (2002) 1681.
[13] D.J. Funk, D.S. Moore, K.T. Gahagan, S.J. Buelow, J.H. Reho, G.L. Fisher, R.L. Rabie, Phys. Rev. B 64 (11) (2001) 115114.
[14] F. Gervais, in: E.D. Palik (Ed.), Handbook of Optical Constants of Solids II, Academic Press, San Diego, 1991, p. 761.
[15] L.M. Barker, R.E. Hollenbach, J. Appl. Phys. 41 (10) (1970) 4208.
[16] N.W. Ashcroft, K. Sturm, Phys. Rev. B 24 (1981) 2315.
[17] R.G. Dandrea, N.W. Ashcroft, Phys. Rev. B 32 (10) (1985) 6936.
[18] S.D. McGrane, D.S. Moore, D.J. Funk, J. Appl. Phys. 93 (9) (2003) 5063–5068.
[19] S.P. Marsh, LASL Shock Hugoniot Data, University of California, Berkeley, 1980.
[20] M. Born, E. Wolf, Principles of Optics, 4th ed, Pergamon Press, New York, 1970.
[21] The phase shifts reported in [16] due to optical changes in the shocked Al are <0.05, making them negligible for the much larger phase shifts discussed here.
[22] J.L. Wise, L.C. Chhabildas, in: Y.M. Gupta (Ed.), Shock Waves in Condensed Matter, Plenum Press, 1985.
[23] L.C. Chhabildas, J.R. Asay, J. Appl. Phys. 50 (1979) 2749.
[24] The shock velocity was estimated from a fit to the change in absorption data vs. time and the propagation time calculated for the 660 nm film.
[25] D.S. Moore, S.D. McGrane, J. Mol. Struc. (2003) (accepted for publication).